Journal of Computer-Aided Molecular Design, 8 (1994) 113–122
ESCOM

J-CAMD 225

A molecular model of the folate binding site of *Pneumocystis carinii* dihydrofolate reductase

William M. Southerland

Department of Biochemistry and Molecular Biology, Howard University, College of Medicine, Washington, DC 20059, U.S.A.

Received 23 March 1993
Accepted 20 July 1993

Key words: Model; *P. carinii*; Dihydrofolate reductase; Methotrexate; Binding site

SUMMARY

The inhibition of *Pneumocystis carinii* dihydrofolate reductase (DHFR) continues to be the major treatment strategy for *P. carinii* pneumonia (PCP). The design of new anti-pneumocystis agents would be significantly enhanced by the availability of a 3D model of the methotrexate (MTX) binding site of the *P. carinii* DHFR. However, an X-ray crystal structure of the *P. carinii* DHFR is not yet available. Alignment of the amino acid sequences of *P. carinii* and *Lactobacillus casei* DHFRs indicates that the two proteins show approximately 80% homology among MTX binding-site residues. This high level of homology suggests that the *L. casei* DHFR MTX binding-site structure could serve as a structural template in developing a model of the *P. carinii* DHFR MTX binding site. Therefore, the X-ray crystal structure of *L. casei* DHFR was used to develop a 3D model of the methotrexate binding site of *P. carinii* DHFR. The molecular modeling and dynamics software QUANTA/CHARMm was used. Amino acid residue mutations and deletions were performed using QUANTA and macromolecular minimizations were achieved with CHARMm. The MTX binding-site residues of *L. casei* DHFR were mutated to the corresponding residues of the *P. carinii* DHFR sequence. The resulting structure was extensively minimized. The resulting *P. carinii* MTX binding-site model showed significant differences in hydrogen-bonding patterns from the *L. casei* MTX binding site. Also, the *P. carinii* site is more hydrophobic than the corresponding *L. casei* site. Analysis of atom-to-atom close contacts between methotrexate and protein binding-site residues indicates that the *P. carinii* MTX binding-site complex is primarily stabilized by hydrophobic interactions, while the *L. casei* complex is mostly stabilized by electrostatic interactions. The model is consistent with the observed increased sensitivity of *P. carinii* DHFR to lipid-soluble inhibitors and provides a rational basis for the design of new anti-pneumocystis agents.

INTRODUCTION

Current treatment strategies of PCP are aimed at inhibiting the *P. carinii* folate synthesis pathway and/or the *P. carinii* dihydrofolate reductase (DHFR) reaction. For example, Bacitrim, which is currently used in the treatment of PCP, consists of the DHFR inhibitor, trimethoprim

and sulfamethoxazole, an inhibitor of folate synthesis. However, trimethoprim only poorly inhibits the *P. carinii* DHFR [1,2] although it shows significant antibacterial and antiprotozoan properties. Another DHFR inhibitor trimetrexate (TMTX), which is an MTX analog, has more recently been used in the treatment of AIDS-associated PCP [3]. TMTX is a much better inhibitor of *P. carinii* DHFR than trimethoprim. Unlike MTX, which requires a mediated transport system to cross cell membranes, TMTX is lipid-soluble and freely diffuses across cell membranes. As a result, TMTX gains equal access to both host and *P. carinii* DHFRs. Therefore, the TMTX treatment strategy involves rescue of host cells with leucovorin.

Since trimethoprim does not show effective anti-pneumocystis properties and TMTX does not significantly discriminate between the *P. carinii* and human DHFRs, the search for an effective and highly selective *P. carinii* DHFR inhibitor continues. Broughton and Queener [4] used *P. carinii* DHFR to screen potential anti-pneumocystis drugs. They observed the following 50% inhibitory concentrations: trimethoprim: 12 μM; TMTX: 42 nM; and pyrimethamine: 3.8 μM. They also observed that, while trimethoprim was the least potent, it was the most selective and TMTX was nonselective. Other drugs were also screened in this study. However, the authors indicated that the most promising compounds were chemically related to MTX. Additionally, Queener [5] also screened analogs of pyrimethamine, methotrexate and trimethrexate for inhibition of *P. carinii* DHFR. The results indicated that one pyrimethamine analog was selective for *P. carinii* DHFR with potency in the micromolar range. Two TMTX analogs and several MTX analogs were found to be selective for *P. carinii* DHFR. These agents all had potencies in the nanomolar range. The data indicate that MTX analogs hold significant promise for treatment of PCP.

Edman et al. [6] have successfully expressed the *P. carinii* dihydrofolate reductase gene in *Escherichia coli*. These investigators observed that trimethoprim is also a very poor inhibitor of the recombinant *P. carinii* DHFR. Analyses of the *P. carinii* genomic sequences predicted a monofunctional enzyme of 206 amino acids (M_r of 23 868). Edman et al. [6] aligned the primary sequences of *P. carinii* DHFR and DHFRs of known 3D structure from *L. casei*, human, *Saccharomyces cerevisiae*, and *Leishmania major*. It was observed that the *P. carinii* DHFR contained those residues that are conserved in all the other DHFRs. Also, the larger size of the *P. carinii* DHFR could be accounted for by insertions in loop regions between secondary structural elements present in DHFRs of known 3D structure. This finding is consistent with the suggestion that *P. carinii* DHFR is likely to consist of a general structural framework that is very

TABLE 1
L. casei METHOTREXATE BINDING-SITE RESIDUES

Residue name	Residue no.	Residue name	Residue no.	Residue name	Residue no.
Phe	49	Ala	6	Pro	24
Phe	30	Val	41	Arg	57
Tyr	29	Ala	97	Thr	34
Arg	31	Thr	116	Pro	55
His	28	Leu	4	Asp	26
Pro	50	Tyr	155	Ser	48
His	18	Leu	114	Trp	5
Leu	19	Leu	27	Phe	103
Thr	45	Ser	54	Gly	98
Trp	21				

similar to that of DHFRs of known structure. More recently, Kovas et al. [7] characterized the DHFRs from both *P. carinii* and *Toxoplasma gondii*. They reported a molecular weight of 26 000 for the *P. carinii* DHFR and showed that the enzyme did not contain any thymidylate synthase activity. These results are in agreement with those reported earlier by Edman et al. [6] for the recombinant *P. carinii* DHFR.

It is clear that the *P. carinii* DHFR is a major target for the development of anti-pneumocystis treatment regimens. However, these studies have been performed in the absence of detailed structural knowledge of the *P. carinii* folate binding site. Such knowledge of the *P. carinii* DHFR binding site would greatly enhance the efficiency of these studies. Thus, we have performed computer-aided molecular modeling studies which resulted in a 3D model of the *P. carinii* DHFR methotrexate binding site.

METHODS

The molecular modeling and dynamics software package QUANTA/CHARMm from Molecular Simulations, Inc. was used in these studies. The X-ray crystal structure of the *L. casei* DHFR/MTX–NADP complex was obtained from the Brookhaven Protein Databank and used as the template in deriving the structure of the *P. carinii* DHFR MTX binding site. The X-ray structure of the *L. casei* DHFR [8] was extensively minimized before modeling techniques were applied. The Adopted-Basis Newton Raphson algorithm in CHARMm was used for structural minimizations, which were carried out for 1000 steps in order to generate a relaxed structure. A distance-dependent dielectric constant was used in the minimizations. After 1000 steps, the root-mean-square (rms) deviation of the minimized protein structure with respect to the starting coordinates was 0.83 Å. The corresponding rms deviations for the backbone and side-chain atoms were 0.64 and 0.97 Å, respectively. Constraints were not used during the minimization. This procedure did

```
L.casei          TAFLWAQDRDGLIGKDGHLPW-HLPDDLHYFRAQTV-----------GKIMV   40
P.carinii   MNQQKSLTLIVALTTSYGIGRSNSLPW-KLKKEISYFKRVTSFVPTFDSFES--MNVVL   56
                  ---          --     - ------ -

L.casei          VGRRTYESFP--KRPLPERTNVVLTHQEDYQAQG-AVVVH----------DV   78
P.carinii        MGRKTWESIPLQFRPLKGRINVVITRNESLDLGNGIHSAK---------S-L   97
                 -   - ---    -- -

L.casei          AAVFAYAKQHPDQ--------ELVIAGGAQIFTAFK-----DDVDTLLVTRL  117
P.carinii        DHALELLYRTYGSESSVQIN-RIFVIGGAQLYKAAMDH---PKLDRIMATII  145
                                      --   -             - -

L.casei          AGSFEGDT-KMIPLNWDDFTKVSS---------------------------  140
P.carinii        YKDIHCDV-FFPLKFRDKEWSSVWKKEKHSD----------LESWVGTKVPH  186

L.casei          RTVEDTNPALTHTYEVWQKKA                                 162
P.carinii        GKINEDG--FDYEFEMWTRDL                                 206
                                -
```

Fig. 1. Sequence alignment of *L. casei* and *P. carinii* DHFR amino acid sequences. Binding-site residues are underlined.

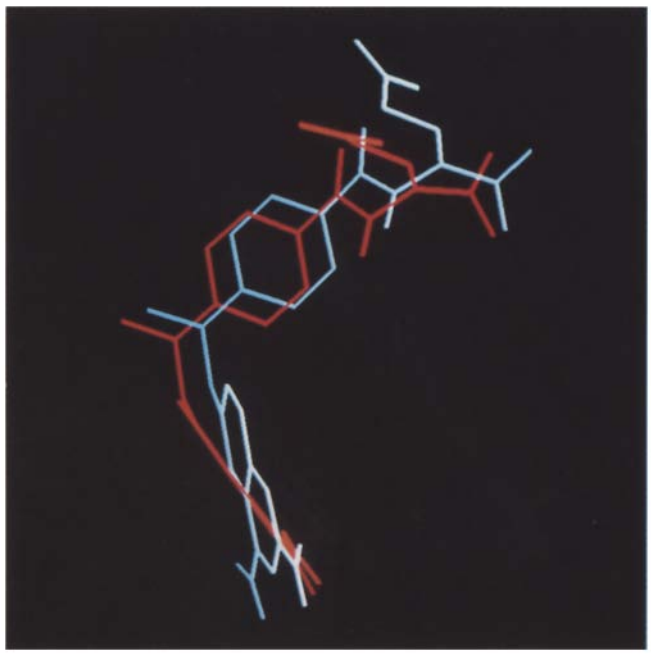

Fig. 2. Conformation of MTX while bound to the *L. casei* DHFR folate site (red) and the modeled *P. carinii* DHFR folate site (blue).

not result in convergence; however, a final gradient of 0.21 kcal/mol/step was observed. The amino acid sequences of *P. carinii* and *L. casei* DHFRs were aligned as described by Edman et al. [6]. The alignment indicated that the overall sequence homology between the two enzymes is approximately 30%, while that for the corresponding MTX binding-site residues is approximately 80%. These findings suggested a very strong likelihood for developing an accurate model of the *P. carinii* DHFR methotrexate binding site.

Using the atom selection facility of CHARMm, all amino acid residues within 5 Å of the MTX component of the *L. casei* DHFR MTX–NADP complex were identified (Table 1). These residues were then compared to the corresponding residues of the *P. carinii* DHFR sequence (Fig. 1). In those instances where the corresponding residues were not identical, the *L. casei* DHFR

TABLE 2
AMINO ACID MUTATIONS REQUIRED TO MODEL THE *P. carinii* DHFR BINDING SITE FROM THE *L. casei* DHFR BINDING SITE

L. casei DHFR binding-site residues → *P. carinii* DHFR binding-site residues	
Phe^{49} → Ile	Leu^{14} → Met
Arg^{31} → Lys	Leu^{27} → Ile
His^{28} → Ser	Pro^{24} → Lys
His^{18} → Ser	Pro^{55} → Lys
Val^{41} → Met	Asp^{26} → Glu
Ala^{97} → Ile	Trp^{5} → Val
Leu^{4} → Ile	Phe^{103} → Tyr
Tyr^{155} → Phe	

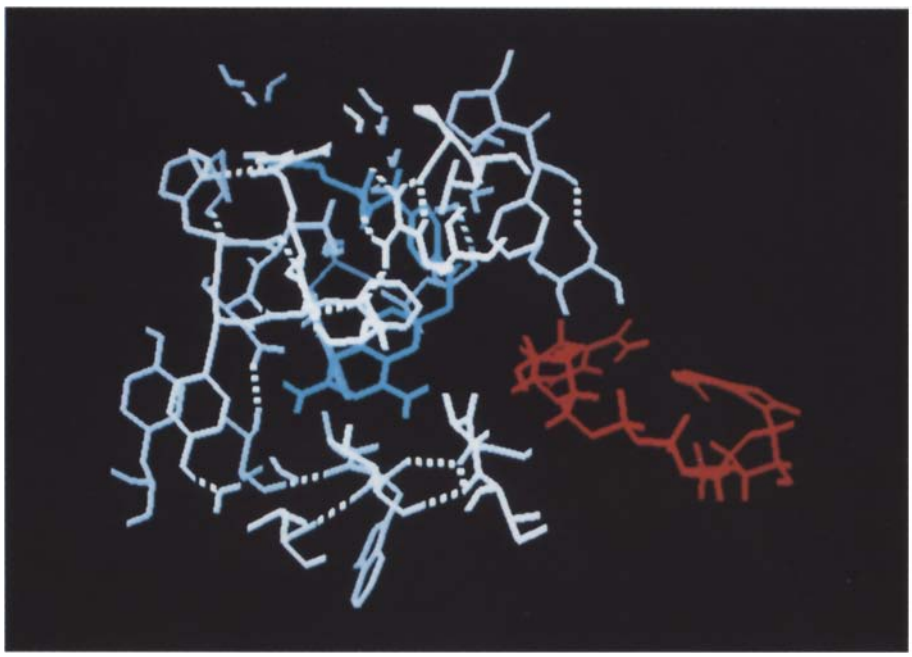

Fig. 3. Folate binding site of *L. casei* DHFR. Light blue represents binding-site residues, dark blue represents bound MTX, and red represents bound NADPH. Hydrogen bonds are indicated by broken white lines.

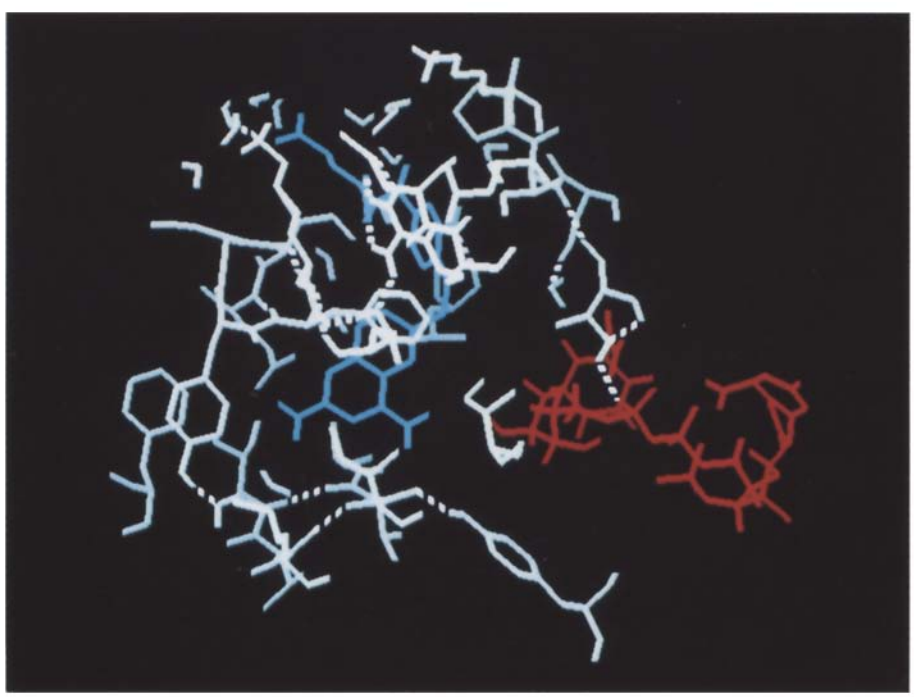

Fig. 4. Modeled folate binding site of *P. carinii* DHFR. Light blue represents binding-site residues, dark blue represents bound MTX, and red represents bound NADPH. Hydrogen bonds are indicated by broken white lines.

residues were altered in order to be identical to the *P. carinii* DHFR residues. The required amino acid changes were performed using the QUANTA mutate facility. Fifteen out of 28 residue positions required changes (Table 2). Consequently, the two binding sites exhibited 13 corresponding sequence positions with identical amino acids. Additionally, 10 of the 15 residue changes required only conservative amino acid replacements. As a result, 23 of the 28 binding-site residues are identical or similar between the two sites, which is consistent with approximately 80% sequence similarity or relatedness.

The amino acid changes resulted in a hybrid DHFR protein, consisting of the *P. carinii* DHFR MTX binding site surrounded by *L. casei* DHFR sequences. This protein was once again extensively minimized as described earlier for the *L. casei* DHFR. After minimization, the MTX binding sites in the hybrid DHFR and the *L. casei* DHFR were analyzed in terms of structure and stability.

RESULTS

Comparison of MTX conformations

First, the conformations of MTX while bound to the *P. carinii* and *L. casei* MTX binding sites were compared (Fig. 2). The two MTX conformations exhibited an overall rms difference of 1.06 Å, which is indicative of differences in atomic coordinates for the two conformations. Thus, the two MTX binding sites require different MTX conformations for optimal binding.

Comparison of overall conformational stabilities of DHFR, MTX and NADP complexes

The potential energy of a molecular structure is sensitive to its conformation. Table 3 shows the potential energy values of the *L. casei* DHFR and the hybrid DHFR containing the modeled *P. carinii* DHFR folate binding site after 1000 steps of minimization. As can be seen, potential energy values were obtained for each DHFR in a variety of states. Binding of MTX alone or MTX and NADP to the *L. casei* DHFR did not lower the potential energy of the structure. However, binding of NADP alone did cause a decrease in energy of approximately 50 kcal/mol. In the case of the modeled *P. carinii* structure, binding of MTX alone or NADP alone caused only very little change in the potential energy of the structure. However, binding of both MTX and NADP resulted in a much larger synergistic lowering of the potential energy of the structure. These results suggest the presence of site-to-site interaction between the MTX and NADP binding

TABLE 3
POTENTIAL ENERGY COMPARISONS OF MINIMIZED DHFRs

Energy (kcal/mol)	MTX	NADP
***L. casei* DHFR**		
−8053.72	−	−
−8053.32	+	−
−8105.71	−	+
−8056.88	+	+
Hybrid DHFR containing the modeled *P. carinii* folate binding site		
−8123.20	−	−
−8129.66	+	−
−8118.76	−	+
−8168.92	+	+

sites of the *P. carinii*-modeled DHFR. This kind of site-to-site interaction was not evident with the *L. casei* DHFR.

Analysis of atom-to-atom contacts

The structures of the *L. casei* and the modeled *P. carinii* MTX binding sites are shown in Figs. 3 and 4, respectively. Tables 4 and 5 show analyses of the close contacts between MTX and the binding-site residues for the *L. casei* and *P. carinii* sites, respectively. The MTX–NADP complexes of the *L. casei* DHFR and the hybrid DHFR containing the *P. carinii* MTX binding site were minimized for 1000 steps prior to the close contact analyses. The *L. casei* site contains a higher number of close atom-to-atom contacts than does the *P. carinii* site. Additionally, in the case of the *L. casei* site, most of the instability for the MTX–binding-site complex is derived from the collective van der Waals repulsive interactions between atom pairs. Most of the instability for the *P. carinii* MTX–binding-site complex is derived from the collective repulsive electrostatic interactions resulting from close atom-to-atom contacts. These results are clarified by a comparison of the total electrostatic and van der Waals energies for the two complexes. The total electrostatic energies for the *L. casei* and *P. carinii* MTX complexes are 5.47 and 9.55 kcal/mol, respectively, while the total van der Waals energies for the two complexes are 6.02 and 4.16 kcal/mol, respectively. Consequently, the collective electrostatic and van der Waals interactions make important but different contributions to the stabilities of the two complexes. Also, the *L. casei*

TABLE 4
L. casei DHFR BINDING-SITE CLOSE CONTACTS

Residue name	Atom name	Residue name	Atom name	Distance (Å)	vdW energy (kcal/mol)	Electrostatic energy (kcal/mol)
Leu^{4}	CD1	MTX	N3	3.26	0.60	0.00
Leu^{4}	O	MTX	NA4	2.80	0.48	23.86
Leu^{4}	O	MTX	HN4B	1.89	0.68	−28.03
Trp^{5}	CA	MTX	N3	3.71	0.01	−2.18
Leu^{19}	CD1	MTX	C7	3.55	0.18	0.00
Asp^{26}	OD2	MTX	NA2	2.96	0.06	24.94
Asp^{26}	OD2	MTX	HN2A	1.98	0.21	−15.66
Leu^{27}	CB	MTX	CG	3.78	0.22	0.00
Leu^{27}	CB	MTX	CD	3.42	0.37	0.00
Leu^{27}	CB	MTX	OE1	3.23	0.22	0.00
Leu^{27}	CG	MTX	CG	3.68	0.52	0.00
Leu^{27}	CD1	MTX	CG	3.87	0.04	0.00
Leu^{27}	CD2	MTX	N8	3.32	0.41	0.00
Leu^{27}	CD2	MTX	C7	3.59	0.12	0.00
Leu^{27}	O	MTX	CB	3.35	0.03	−1.09
His^{28}	ND1	MTX	OE2	2.96	0.06	10.49
Phe^{30}	CD2	MTX	C4A	3.31	0.04	0.00
Phe^{30}	CD2	MTX	C4	3.37	0.07	0.00
Arg^{31}	CA	MTX	O1	3.33	0.16	−3.26
Arg^{31}	CB	MTX	O1	3.34	0.04	0.00
Pro^{50}	CD	MTX	C12	3.60	0.16	0.00
Arg^{57}	NH1	MTX	O1	2.71	0.86	18.05
Arg^{57}	HH11	MTX	O1	1.75	0.45	−21.64
Total					6.02	5.47

TABLE 5
P. carinii DHFR BINDING-SITE CLOSE CONTACTS

Residue name	Atom name	Residue name	Atom name	Distance (Å)	vdW energy (kcal/mol)	Electrostatic energy (kcal/mol)
Ile^{4}	CG1	MTX	N3	3.30	0.51	0.00
Ile^{4}	O	MTX	HN4B	2.06	0.06	−25.70
Val^{5}	CA	MTX	NA4	3.61	0.074	−3.36
Glu^{26}	CG	MTX	N1	3.40	0.27	4.06
Ile^{27}	CG2	MTX	CG	3.82	0.12	0.00
Ile^{27}	CG1	MTX	CG	3.91	0.05	0.00
Ile^{27}	CD	MTX	C7	3.48	0.32	0.00
Phe^{30}	CD1	MTX	C16	3.35	0.21	0.00
Phe^{30}	CD2	MTX	C8A	3.38	0.00	0.00
Phe^{30}	CE1	MTX	C16	3.40	0.12	0.00
Lys^{31}	CA	MTX	O1	3.19	0.46	−3.41
Lys^{31}	CG	MTX	CT	3.61	0.05	0.00
Ile^{49}	CG1	MTX	C12	3.74	0.02	0.00
Pro^{50}	CD	MTX	C12	3.61	0.14	0.00
Arg^{57}	NH1	MTX	O1	2.66	1.19	18.39
Arg^{57}	HH11	MTX	O1	1.82	0.21	−20.92
Arg^{57}	NH2	MTX	O2	2.97	0.06	12.64
Ile^{97}	CG1	MTX	NA4	3.52	0.09	0.00
Thr^{116}	OG1	MTX	NA2	2.88	0.21	27.85
Total					4.16	9.55

DHFR MTX binding-site close contact region consists of four charged amino acids and six nonpolar amino acids. The corresponding *P. carinii* site consists of three charged amino acids, one uncharged polar amino acid and seven nonpolar amino acids. Consequently, it is clear that the *P. carinii* site is a more hydrophobic environment than the *L. casei* site. Another interesting feature of the two sites is the differing contribution made by the residue in position 27. In the *L. casei* site, Leu^{27} significantly contributes to the interaction between the MTX and the binding site, participating in eight atom-to-atom contacts. The corresponding residue in the *P. carinii* site is Ile^{27}, which makes only three atom-to-atom contacts. This number of contacts is more commensurate with the number of contacts exhibited by other close contact residues.

Table 6 shows the distance analysis of the DHFR MTX binding site–MTX complexes. As can be seen, the average distance between MTX atoms and the binding-site atoms is shorter in the *L. casei* complex than the corresponding distance in the *P. carinii* complex. This analysis suggests that the *L. casei* binding site is smaller than the *P. carinii* binding site. Consequently, the average van der Waals repulsion forces are also larger for the *L. casei*–MTX complex. As a result, it is not surprising that addition of MTX to the *L. casei* enzyme does not lead to a more stable

TABLE 6
DISTANCE ANALYSIS OF MTX BINDING SITES

	Average distance between DHFR and MTX (Å)	Average vdW repulsion forces (kcal/mol)	Total vdW repulsion forces (kcal/mol)
P. carinii	3.25	0.22	4.16
L. casei	3.16	0.26	6.02

TABLE 7
HIGH-ENERGY CONTACTS BETWEEN THE *P. carinii* ACTIVE SITE AND METHOTREXATE

Residue name	Atom name	Atom charge	Residue name	Atom name	Atom charge	Distance (Å)	vdW energy (kcal/mol)	Electrostatic energy (kcal/mol)
Glu^{26}	CG	−0.36	MTX	N1	−0.26	3.40	0.27	4.06
Arg^{57}	NH1	−0.45	MTX	O1	−0.32	2.66	1.19	18.39
Arg^{57}	NH2	−0.45	MTX	O2	−0.25	2.97	0.06	12.64
Thr^{116}	OG1	−0.65	MTX	NA2	−0.37	2.88	0.21	27.85

conformation (Table 3).

In both MTX binding-site structures, atom-to-atom contacts with unfavorable electrostatic interactions are associated with large positive values for electrostatic energies. However, in each binding site, these unfavorable contacts are mostly compensated by other favorable atom-to-atom contacts with large negative values for electrostatic interaction energies.

DISCUSSION

A 3D model of the *P. carinii* DHFR MTX binding site (Fig. 4) has been developed using the corresponding structural region from the X-ray crystal structure of *L. casei* DHFR. Analysis of sequence alignments of *L. casei* and *P. carinii* sequences [6] revealed approximately 80% sequence homology between the MTX binding sites of the two DHFRs. However, the modeled *P. carinii* MTX binding site appears to be significantly more hydrophobic than the *L. casei* site. This observation is consistent with the observation that the lipid-soluble compounds TMTX and pyrimethamine are much better inhibitors of *P. carinii* DHFR than more polar compounds such as trimethoprim [4–6]. The structure of the *P. carinii* DHFR MTX binding-site model reported here provides a chemical basis for the enhanced interaction of lipid soluble compounds with the *P. carinii* DHFR active site.

Another interesting difference between the *L. casei* and *P. carinii* DHFR MTX binding sites is the role of the residue in position 27. In the *L. casei* site, the leucine in this position participates in eight atom-to-atom close contacts. This number of contacts suggests that Leu^{27} may be serving as a platform to which the MTX is anchored. On the other hand, the role of Ile^{27} is not as significant in the *P. carinii* site. This comparison suggests that the MTX contacts are more evenly distributed in the *P. carinii* site.

Finally, *P. carinii* DHFR continues to be a prominent therapeutic target in the treatment of PCP. However, detailed structural knowledge of the *P. carinii* DHFR MTX binding site has not

TABLE 8
PROPOSED ATOM CHANGES FOR NEW DRUG DESIGN

Residue name	Atom name	Original atom type	Description of original atom type	Proposed new atom type	Description of new atom type
MTX	N1	N6R	Aromatic nitrogen	C6R	Aromatic carbon
MTX	O1	OC	Charged oxygen	NP	Peptide/amide nitrogen
MTX	O2	OC	Charged oxygen	NP	Peptide/amide nitrogen
MTX	NA2	NP	Peptide/amide nitrogen	CT	Aliphatic carbon

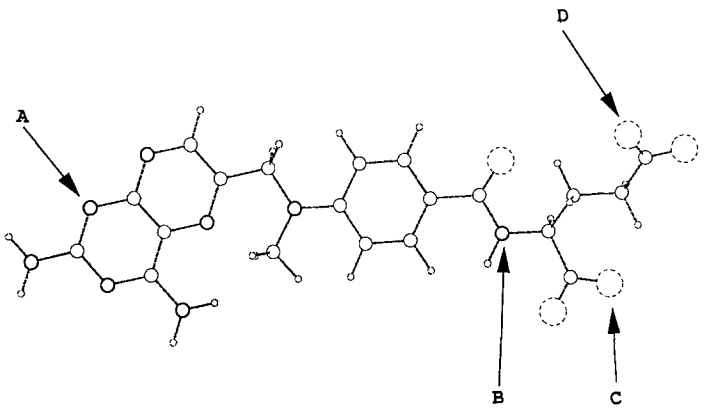

Fig. 5. Ball-and-stick drawing of methotrexate. Arrows indicate positions of proposed atom changes. (A) atom type N6R → C6R; (B) atom type NP → CT; (C and D) atom type OC → NP.

been available to contribute to the design of agents specific for the inhibition of *P. carinii* DHFR. Examination of the atom-to-atom contacts for the *P. carinii* DHFR (Table 5) reveals the presence of four atom-to-atom contacts with clearly unfavorable electrostatic energies of interaction. These unfavorable contacts are listed in Table 7 with partial atomic charges indicated. It is clear that an MTX analog in which the electrostatic energy of one or each of these contacts could be lowered would result in enhanced binding of the analog to the *P. carinii* binding site. Such changes in the MTX structure would likely result in an MTX analog that is also more hydrophobic (Table 8). Changes identified in Table 8 are illustrated in Fig. 5. Moreover, the model of the *P. carinii* DHFR binding site presented here is consistent with observed inhibition of *P. carinii* DHFR by hydrophobic MTX analogs and suggests that hydrophobicity should be a significant consideration in the design of new agents for the inhibition of *P. carinii* DHFR.

CONCLUSIONS

The 3D structure of the *P. carinii* DHFR MTX binding site has been modeled. The structure is significantly hydrophobic, which is consistent with the experimentally observed enhanced inhibition of *P. carinii* DHFR by lipid soluble agents. The model also provides a rational basis for the incorporation of hydrophobic properties into the design of new anti-pneumocystis agents.

REFERENCES

1 Allegra, C.J., Kovacs, J.A., Drake, J.C., Swan, J.C., Chabner, B.A. and Masur, H., J. Exp. Med., 165 (1987) 926.
2 Ansden, G.W., Kowalsky, S.F. and Morse, G.D., Annu. Pharmacother., 26 (1992) 218.
3 Kovacs, J.A., Allegra, C.J., Beaver, J., Boarman, D., Lewis, M., Parrill, J.E., Chabner, B. and Masur, H., J. Infect. Dis., 160 (1989) 312.
4 Broughton, M.C. and Queener, S.F., Antimicrob. Agents Chemother., 35 (1991) 1348.
5 Queener, S.F., J. Protozool., 38 (1991) 1545.
6 Edman, J.C., Edman, U., Cao, M., Lundgran, B., Kovacs, J.A. and Santi, D.V., Proc. Natl. Acad. Sci. USA, 86 (1989) 8625.
7 Kovacs, J.A., Allegra, C.J. and Masur, H., Exp. Parasitol., 71 (1990) 60.
8 Matthews, D.A., Alden, R.A., Bolin, J.T., Filman, D.J., Freer, S.T., Hamlin, R., Hol, W.G.J., Kisliuk, R.L., Pastore, E.J., Plante, L.T., Xuong, N.-H. and Kraut, J., J. Biol. Chem., 253 (1978) 6946.